TITLE: Reprogramming of energetic metabolism: increased expression and roles of pyruvate carboxylase in papillary thyroid cancer

AUTHORS:

Dr. Strickaert Aurélie [1] astricka@ulb.ac.be, +3225554160

Dr. Corbet Cyril [2] cyril.corbet@uclouvain.be , +3227645248

Mr. Spinette Selim-Alex [3] selim-alex.spinette@bordet.be

Dr. Craciun Ligia [3] ligia.craciun@bordet.be,

Dr. Dom Geneviève [1] genevieve.dom@ulb.ac.be, +3225554140

Pr. Andry Guy [4] guy.andry@bordet.be,

Pr. Larsimont Denis [3] denis.larsimont@bordet.be,

Pr. Wattiez Ruddy [5] ruddy.wattiez@umons.ac.be,

Pr. Dumont Jacques E. [1] jedumont@ulb.ac.be, +3225554134

Pr. Feron Olivier [2] olivier.feron@uclouvain.be, +3227645264

Pr. Maenhaut Carine [1] cmaenhau@ulb.ac.be, +3225554137

AFFILIATIONS :

[1] Institute of Interdisciplinary Research (IRIBHM), Université libre de Bruxelles (ULB), 808 route de Lennik 1070 Brussels, Belgium.

[2] Pole of Pharmacology and Therapeutics, Institut de Recherche Expérimentale et Clinique (IREC), Université catholique de Louvain (UCL), Avenue Hippocrate 55, boîte B1.55.02, 1200 Brussels, Belgium.

[3] Department of Pathology, Jules Bordet Institute, Université libre de Bruxelles, 121-125, boulevard de Waterloo – 1000 Brussels, Belgium.

[4] Thoracic Surgery, Jules Bordet Institute, Université libre de Bruxelles (ULB), Boulevard de Waterloo, 125-1000 Brussels, Belgium

[5] Proteomics and Microbiology Laboratory, Research Institute for Biosciences, Université de Mons, 20, place du Parc, B7000 Mons, Belgium.

RUNNING TITLE: Energetic metabolism in Papillary thyroid cancer

KEYWORDS: Papillary Thyroid Cancer, Energetic metabolism, TCA cycle, Anaplerosis, Pyruvate carboxylase, Heterogeneity, Tumor microenvironment, CAFs, Reverse Warburg effect

ABSTRACT

Background: Energetic metabolism is described to be deregulated in cancer and the Warburg effect is presented as a major hallmark. Recently, cellular heterogeneity in tumors and tumor microenvironment have been recognized to play an important role in several metabolic pathways in cancer. However, their contribution to papillary thyroid cancer (PTC) development and metabolism is still poorly described.

Methods: We performed a proteomic analysis of 5 PTC and investigated the cellular distribution of several upregulated metabolic proteins in the cancer and in the stromal cells of PTC.

Results: MS/MS analysis revealed the upregulation of many metabolism-related proteins, among which pyruvate carboxylase. Pyruvate carboxylase knockdown in thyroid cell lines alters their proliferative and motility capacities, and measurements of oxygen consumption rates showed that this enzyme is involved in the replenishment of the TCA cycle.

Immunostainings of several upregulated metabolic proteins showed that thyroid cancer cells have an increased mitochondrial oxidative metabolism compared to stromal cells.

Conclusion: PTC have a very active TCA cycle, continuously replenished by a pyruvate carboxylase mediated anaplerosis. This is specifically observed in the tumor cells.

MAIN BODY:

INTRODUCTION

Deregulated energetic metabolism is one of the hallmarks of cancer, playing a crucial role in tumor development (1–3). Tumor cells have high energetic requirements to support many biosynthesis pathways and promote cell growth. The Warburg effect has been proposed for a long time to be the major metabolic reprogramming in cancer. In this scheme, glucose uptake is increased, metabolized to pyruvate, then transformed into lactate, instead of entering the TCA cycle, even when the level of oxygen is normal in the tumor microenvironment (4). This allows the oxidation of the NADH produced by glycolysis into NAD^+ sustaining glycolytic flux (4, 5). Since a few years, another concept is emerging: the TCA cycle would maintain its functions and participate to the synthesis of energy and biosynthetic intermediates as metabolic precursors out of the mitochondria (6). In addition, the metabolism of cancer cells is influenced by the metabolic microenvironment of the tumor. Indeed, several studies have described for example the important role of cancer-associated fibroblasts (CAFs) in the majority of tumors (7). They contribute to tumor proliferation by exchanging cytokines, growth factors or pro-angiogenic factors (8, 9), but it is still unclear how they are involved in tumor metabolism. Recent studies showed that CAFs carry out aerobic glycolysis and release lactate in the tumor microenvironment (10), then available for the cancer cells sustaining an oxidative mitochondrial metabolism (11). This model, named “The Reverse Warburg Effect”, allows exchanging resources between cells inside tumors and defines CAFs as feeders of lactate, later transformed into pyruvate by oxidative tumor cells in order to replenish the TCA cycle.

The TCA cycle intermediates replenishment, or anaplerosis, is known to be assumed by two major pathways: (1) glutaminolysis, which consists in using glutamine, metabolized to glutamate by glutaminase (GLS), itself converted into α-ketoglutarate by glutamate dehydrogenase (GDH); (2) the carboxylation of pyruvate to oxaloacetate via ATP-dependent pyruvate carboxylase (PC). In cancers, a compensatory relationship between GLS and PC was

shown when cells deprived of glutamine switched to a glucose-dependent anaplerosis via pyruvate (12). At the opposite, intracellular lactate signaling promotes glutamine uptake, that becomes the major substrate (13).

Thyroid cancer is the most frequent endocrine cancer in human, and papillary thyroid carcinoma (PTC) represents up to 85% of all malignant thyroid tumors. PTC is usually biologically indolent and has an overall 5- to 10-years survival rate of 80–95%. Present therapy is based on thyroidectomy followed by a radioiodide treatment. The most dedifferentiated cases among PTC are associated with treatment resistance and cancer recurrence. Several cancers have been metabolically characterized to define new therapeutic approaches using inhibitors against metabolic enzymes. For instance, Doherty et al. developed inhibitors against the lactate dehydrogenase (LDH) proteins, like gossypol or galloflavin (14). Accordingly, characterizing the energetic metabolism of PTC could offer an opportunity to treat its most aggressive forms. For now, thyroid tumor metabolism has been poorly described but appeared to vary according to the histological subtype (15). An increased level of labelled glucose consumption by poorly differentiated thyroid tumors compared to differentiated tumors has been reported, with a strong correlation with the presence of BRAF mutation (16). The enhanced glucose metabolism was validated by the demonstration of the overexpression of glucose transporters 1 and 3 (GLUT1, GLUT3), and of hexokinase 2 (HK2) in BRAF-mutated PTC (17, 18). The expression levels of GLS and of GDH were also increased in BRAF-mutated PTC, suggesting an overall increase in glutamine metabolism (15).

On the other hand, the role of tumor microenvironment is now recognized to play a major metabolic role in a lot of cancers (19, 20). However, its contribution to thyroid tumor development is still poorly described. The cellular heterogeneity of PTC resulting in part from the presence of CAFs has been characterized and revealed a positive correlation with tumor

aggressiveness (21). Another study showed respective overexpression of monocarboxylate transporters 1 and 4 (MCT1, MCT4) in cancer and stromal cells, each one being responsible of lactate transport across the plasma membrane (22).

In this study, we performed a proteomic analysis of PTC, which revealed the upregulation of a high number of metabolism-related proteins. We first focused on pyruvate carboxylase whose expression and functional role were studied in thyroid tumors and in thyroid cell lines. We then extended our study by investigating the expression and cellular localization of other metabolic enzymes. Our data show that PTC have a very active TCA cycle, continuously replenished by a pyruvate carboxylase mediated anaplerosis. This is specifically observed in the tumor cells.

MATERIAL AND METHODS:

Cell culture

Human thyroid cancer cell lines TPC1 (RET/PTC1 rearranged) and 8505C ($BRAF^{V600E}$ and TP53 mutated) (23), and HTori-3 (SV40-immortalized human thyrocytes) (24) were cultured in RPMI 1640 (+ L-glutamine + 25mM Hepes) (Life Technologies) supplemented with 10% FBS, 2% streptomycin/penicillin and 1% amphotericin B (Life Technologies). The cells were grown at 37°C in a humidified atmosphere with 5% CO_2 and 20% O_2. STR analyses performed previously for TPC1 and 8505C cells (25) showed that they were identical to those published by Schweppe et al (26). STR analysis of HTori-3 cells is provided in Supplementary Figure. Their genotype is identical to the STR profile of Nthy-ori 3-1, a subclone of HTori-3 (European Collection of Cell Culture-ECACC 90011609), except a heterozygosity detected for THO1. Moreover these cells express TTF1 and PAX8, suggesting that they are of thyroid origin.

Thyroid tissue samples

Paired samples of normal and tumor thyroid tissues were obtained from patients undergoing surgery for papillary thyroid cancer (n=28). All the tissues were provided by the Anatomical Pathology Department of the J. Bordet Institute (Brussels, Belgium) where the diagnoses were made by pathologists. 5 paired samples, containing at least 70% of tumor cells, were selected for MS/MS and transcriptomic analyses, and the remaining samples were used for validation. Tissue samples were embedded in OCT and directly stored at −80°C until processing. Paraffin sections were used for immunostaining (n=6). Protocols have been approved by the Ethics Committee of the J. Bordet Institute.

MS/MS analysis

Five PTC (classical variant) and their normal adjacent tissues were analyzed by mass spectrometry. All of them carried the BRAF V600E mutation, the most common mutation in PTC (relevant clinical data are provided in Supplementary Table 1). Protein extraction and analysis were performed at the proteomic platform of Professor Rudy Wattiez (University of Mons), with the TripleTOF mass spectrometer (ESI sources). Proteins were identified with the UniProt database.

RNA purification

Total RNA was extracted from thyroid samples or from thyroid cell lines using a TRIzol Reagent kit (Invitrogen Carlsbad, CA, USA) followed by purification on RNeasy columns (Qiagen Hilden, Germany). RNA concentrations were spectrophotometrically quantified, and their integrity was verified using an automated electrophoresis system (Experion, Bio-Rad).

Affymetrix microarray hybridization

The 5 samples analyzed by mass spectrometry and 3 additional samples for which no proteins were available were analyzed by Affymetrix microarrays. RNA amplification, cDNA synthesis and labelling were performed according to manufacturer's instructions (Affymetrix Santa Clara, CA, USA). RNA (100 ng for each sample) from 8 PTC and their normal, non-neoplastic adjacent thyroid tissues were hybridized on Affymetrix Human Genome U133 Plus 2.0 Arrays. CEL file data were normalized by GCRMA (GenePattern - http://www.broad.mit.edu/cancer/software/genepattern/). For each spot, data were expressed as the log2 ratio of fluorescence intensities from tumor and normal tissues.

Quantitative RT-PCR for pyruvate carboxylase mRNA expression

RNA extraction from tissue samples and cell lines was carried out according to manufacturer's instructions (Invitrogen Carlsbad, CA, USA). RNA samples were treated by "DNase I amplification Grade" and subjected to reverse transcription using "Superscript II RNase H Reverse Transcriptase". Pyruvate carboxylase mRNA expression was quantified on an Applied Biosystems 7500 Fast Real Time PCR with SyberGreen (Eurogentec, Liège, Belgium), using oligonucleotides designed with Primer Blast (forward sequence: 5'-GGCGACGGCGAGGAGATAG-3', reverse sequence: 5'- GAGTAGATGGCTACGGTGCG-3'). NEDD8 and TTC1 mRNA expressions were used for normalization (27).

Protein extraction

Thyroid tissues or cells were lysed in Laemmli lysis buffer, supplemented by phosphatase and protease inhibitors (NaF, Vanadate, Pefabloc, Leupeptin and Tablet Roche Inhibitor 25x (Roche Applied Science)). Protein extracts were denatured at 100 C° for 3 min and then quantified by the PAR/IDCR method (Thermo Fisher Scientific Waltham, MA, USA).

Western blotting

Proteins samples (30 µg/well) were loaded on a 7.5% acrylamide gel and run for 1h30 at 20mA/gel. The proteins were transferred to a nitrocellulose membrane at 80V during 1h30. The membrane was first blocked 1 hour at room temperature in Odyssey/PBS (v/v), and then incubated overnight at 4°C with the primary antibody [1:200 anti-PCB rabbit polyclonal antibody, Santa-Cruz (sc-67021); 1:100 anti-PDHE1α mouse monoclonal antibody, Santa-Cruz (sc-377092); 1:5000 anti-GLS rabbit monoclonal antibody, Abcam (ab156876)] in the solution (Odyssey/PBS (v/v) + Tween 0.1%). After incubation for 1 hour in the dark at room temperature with the secondary antibody solution (Odyssey/PBS (v/v) + Tween 0.1% + SDS 0.001%), images were acquired using the Azure Biosystems C500.

Immunostainings

Immunohistochemical analyses were performed on 10 µm thick sections prepared from paraffin-embedded tissues. Expression of smooth-muscle actin was analyzed by pathologists from the J. Bordet Institute to identify CAFs from cancer cells. The sections were deparaffinized, rehydrated, treated with citrate buffer (10 mM, pH6, 95°C, 1h) for antigen retrieval, and their endogenous peroxidase activity was blocked. The sections were then incubated with the primary antibody [anti-PCB (Santa Cruz; sc-67021), anti-PDK (Santa Cruz; sc-28783), anti-PCCB (Abcam; ab96729), anti-ECH1 (Abcam; ab153720), anti-GLS (Abcam; ab156876), anti-LDHA (Abcam; ab47010), anti-LDHB (Santa Cruz; sc100775), anti-MCT1 (Santa Cruz; sc365501), anti-MCT4 (Santa Cruz; sc50329), anti-PCK2 (Abcam; ab137580)] and the detection was performed with the substrate of peroxidase AEC (K3464, DAKO). The primary antibody [anti-PDHα1 (Santa Cruz; sc-377092)] was revealed by immunofluorescence using Alexa Fluor (594nm) (no antibody available for IHC). As negative controls, immunostainings were carried out in the absence of primary antibodies.

siRNA transfection

For transient gene knock-down, a PC-specific siRNA (siPC) sequence (s10089, Ambion) was transfected into different thyroid cell lines (TPC1, HTori-3 and 8505C) using lipofectamine RNAiMAX reagent according to manufacturer's instructions (LifeTechnologies Carlsbad, CA, USA). An unrelated, non-targeting, siRNA (siCTRL) sequence (4390843, Ambion) was used as a negative control. Cells (2 x 10^5/well) were seeded in 6-well plates and transfected 24h later with 25 pmol of siRNA. RNA and protein samples were prepared 48h and 72h post-transfection, respectively.

Proliferation assays

Cell proliferation rate was assessed using the Click-It® Plus EdU Flow Cytometry Assay kit (Thermo Fisher Scientific Waltham, MA, USA) according to manufacturer's instructions. Briefly, cells (75 000 cells/well) were seeded in 12-well plates 24h post-transfection. After 48h, they were incubated for 6h with 10 µM 5, 5-ethynyl-2'-deoxyuridine (EDU). After a final incubation with Alexa Fluor 488-containing buffer, EDU incorporation was analyzed by flow cytometry on the BD LSRFortessa™ cell analyzer.

Migration / Invasion tests

Forty-eight hours post-transfection, cells were incubated in a serum-free medium for 24h. They were plated in migration or invasion chambers (20 000 cells/chamber – 8 µm pore size) (Corning Biocoat Matrigel Invasion Chamber Kit, Corning) with 10% FBS in the lower chamber, as a chemoattractant, and then incubated for 22h. Cells were removed from the upper part with a cotton swab, and cells that have crossed the membrane were stained with the Diff-

Quick Stain Kit (Polysciences Hirschberg, Germany) and 5 fields were counted on the ZOE cell imager.

Metabolic profiling

Oxygen-consumption rate (OCR) was measured using the Seahorse XF96 plate reader (Agilent Technologies). As mentioned above, the cells were routinely cultured in RPMI 1640. This medium contains 11.11 mM D-glucose. For respirometry experiments, cells (5000 cells/well in 96-well plates) were transfected as described above and then incubated (24h post-transfection) in a substrate-free DMEM medium (DMEM D5030, Sigma) for 24h before OCR measurements. Metabolic substrates were given to the cells at 10 mM per well 1 hour before measurements: glucose, lactate, pyruvate, or glucose + glutamine. Where indicated, cells were treated with 10 µM BPTES (Bis-2-(5-phenylacetamido-1,2,4-thiadiazol-2-yl) ethyl sulfide) to inhibit glutaminase activity. Substrate-induced OCR was evaluated by calculating the difference of OCR values before and after substrate addition in each experimental condition.

Statistical analyzes

Results are expressed as mean ± SD with statistical parametric t-tests for in vitro experiments, and as median ± quartiles with statistical non-parametric Mann-Whitney tests for in vivo experiments, of at least three independent experiments, unless otherwise noted. All statistical analyzes were performed with GraphPad Prism 6.01 version. Sample sizes (n) are reported in the corresponding figure legends.

RESULTS:

MS/MS analysis revealed a lot of metabolism-related proteins with deregulated expression.

Five BRAF mutated PTC and their normal adjacent tissue were analyzed by mass spectrometry. The clinical data, mutational status and patient information are given in Supplementary Table 1. The analysis identified about 1100 proteins in paired tumor and normal tissues. Each protein was quantified by calculating the expression ratio in log2 (tumor/normal) and was selected if this ratio was $\geq |1|$. A total of 85 proteins showed deregulated expression in the 5 PTCs (Supplementary Table 2), SH3BP4 being the only one downregulated in all of them. 84 proteins were upregulated, among which several proteins involved in cellular energetic metabolism. We identified proteins involved in the TCA cycle: SUGLG2, PDHA1, CS, PC; in fatty acid β-oxidation: ACADVL, HADH2, DECR1, DCI, PCCA, ECH1; in amino acids degradation: AK2, LONP1, IVD, HIBADH, HIBCH; in ATP production and oxidative stress protection: ATP5B, ATP5L, PRDX3, SOD2; and mitochondrial membrane proteins: CH3CH3, VDAC1, VDAC2. The discovery of the upregulation of PC in papillary thyroid carcinomas, implicated in the oxidative mitochondrial metabolism through its anaplerotic role in replenishing the TCA cycle, led us to explore the expression of other metabolic proteins in PTC (Figure 1). Most of them showed increased protein levels. This was particularly striking for the TCA cycle enzymes. PTC-c appeared to be the most active in terms of metabolism. Indeed, all the investigated proteins were overexpressed at least two times in this sample. PGK1 was downregulated but this was not verified in the 4 other PTC. PTC-a appeared as the less metabolically altered tumor with the smaller number of deregulated proteins, especially for the glycolysis pathway. PTC-e was mainly altered in TCA cycle enzymes and in the "others" metabolic proteins category while glycolysis enzymes showed only a few deregulations. Although the low number of samples does not allow to have sufficient statistical power, our data suggest there might be a correlation between the metabolic profiles and the TNM staging for each one of the PTC examined. For example, PTC-c, which is the most metabolically deregulated, presented a TNM stage of

pT4aN1a, while PTC-a was classified as pT1bN0 (Supplementary Table 1). Of course, this trend should be confirmed with a higher number of samples.

As a complementary approach to evaluate the expression pattern of metabolic proteins in PTC, we performed Affymetrix gene expression analyzes on the same 5 PTC analyzed by mass spectrometry and on 3 additional PTC. A heatmap of the mRNA levels for different metabolic proteins following Affymetrix microarray analysis is presented in Figure 2. There was no correlation between proteomic and transcriptomic expression levels: an overall increase in mRNA expression of proteins involved in glycolysis and inversely an overall decrease in mRNA expression of proteins of the TCA cycle were noticed, with some exceptions. For instance, PC mRNA was strongly overexpressed in the tumors and was even the most overexpressed mRNA among all the genes investigated. The mRNA of the enzymes from the "others" metabolic pathways category showed variable deregulated expressions depending on the gene considered. This lack of correlation has already been reported and reflects different levels of regulation during protein synthesis, e.g. posttranscriptional, translational, or posttranslational regulation (28).

Pyruvate carboxylase expression is increased in PTC.

Among the proteins identified by proteomic analysis, PC was consistently upregulated in all the PTC investigated (Figure 1). Similarly, an increase at the mRNA level was found in the same samples and in three additional PTC (Figure 2), as well as in 49 independent PTC analyzed previously, with a mean ratio in log2 of 1.7 (data not shown) (29). The upregulation of PC mRNA expression has been validated by qRT-PCR in 12 independent PTC: 9 were compared to their normal adjacent tissues (Figure 3a) and 3, for which no adjacent tissue was available, were compared to a pool of 22 normal thyroid tissues (Figure 3b). PTC9 has been compared both to its normal adjacent tissue and to the pool of normal thyroids, which explains the

difference between PC mRNA relative expressions. The mean of expression (log2 of expression ratios between tumor and normal tissues) was 1.75, and 9/12 PTC showed a more than 2 fold upregulation. Increased protein expression of PC has been validated by Western blotting (Figure 3c) on 4 samples already tested for mRNA expression (PTC1-4) and on 11 additional samples. Altogether, these data provided good evidence that PC was upregulated in PTC and this led us to further explore its function in thyroid cancer cells.

Pyruvate carboxylase knockdown in thyroid cell lines alters their proliferative and motility capacities.

Three thyroid cell lines (TPC1, 8505C, HTori-3) were used to investigate the functional role of PC, following siRNA transfection. PC mRNA expression level was significantly decreased 48 hours following siPC transfection in TPC1 cells (Figure 4a), and the downregulation of the protein was validated by Western blotting (Figure 4b) in the three cell lines, 72 hours after transfection. PC protein levels were measured in cells transfected with siPC, with siCTRL, and in non-transfected cells. No difference was observed between non-transfected cells and cells transfected with siCTRL, whereas PC expression was clearly downregulated following siPC transfection.

PC knockdown was accompanied by changes in the proliferative capacity of TPC1 and 8505C cells (Figure 4c). After 72 hours of transfection, there was no change in the proliferation rate when the cells were transfected with the siCTRL compared with non-transfected cells, while siPC transfection markedly reduced the percentage of EdU positive cells for TPC1 and less importantly for 8505C. There was no statistical difference in the percentage of EdU labelled cells for HTori-3 cells.

We next investigated the role of PC on the migration and invasion properties of the three cell lines. These were evaluated by using migration or invasion chambers and by counting the cells

which had crossed the specific membranes. SiPC transfection altered the migration and/or the invasion abilities of the cells: the number of migrating cells was reduced by one half for the 3 cell lines after transfection of siPC (Figure 4d), and the number of invading cells decreased about 4 times for TPC1 cells, and about 2 times for 8505C cells. No effect on invasion was observed in HTori-3 cells (Figure 4e).

Pyruvate carboxylase is involved in the replenishment of the TCA cycle in thyroid cell lines.

The three cell lines were then used to investigate the role of PC in energetic cancer metabolism (Figure 5). We used the Seahorse Technology to measure O_2 consumption rates (OCR), and different substrates were given to the cells to evaluate their contribution to the oxidative metabolism: glucose, lactate, pyruvate, glucose + glutamine, or glucose + glutamine +/- BPTES, a glutaminase inhibitor. O_2 consumption was higher when siCTRL transfected cells received lactate or pyruvate than glucose and was even more important with glucose + glutamine, suggesting that glutamine is a central nutrient for anaplerosis in the 3 cell lines. The OCR was markedly reduced following siPC transfection regardless of the substrate, suggesting that PC participates in the replenishment of the TCA cycle. Despite the lower level of PC expression in HTori-3 cell line than in the 2 other cell lines (Figure 4b), we also observed a decrease of OCR in these cells. This was less the case when the cells were fed with glucose + glutamine, suggesting that glutamine alone is sufficient. To understand how the cells were taking advantage of anaplerotic resources, we treated them with BPTES. This treatment did not affect O_2 consumption in siCTRL transfected cells, but strongly decreased it in PC knockdown cells. This suggests that PC and GLS are codependent, i.e. if one of the 2 major anaplerosis pathways is affected, the other takes over.

Thyroid cancer cells have an increased oxidative metabolism compared to stromal cells

The overexpression of pyruvate carboxylase in PTC and its participation in the replenishment of the TCA cycle, coupled with the increased expression of many other metabolic proteins, suggests an increased oxidative metabolism in this tumor type. However, PTC are heterogeneous tumors containing stromal cells, mainly CAFs, and we have previously shed light on the important role of this stroma in tumor expansion (Tarabichi et al, 2018). Within this context, since our "omic" studies were performed with bulk tissues, we decided to investigate the cellular distribution of several upregulated metabolic proteins in the cancer and in the stromal cells of PTC, and more specifically their expression in CAFs. We performed immunostainings of PC, PCK2, PDHα1, GLS, ECH1, PCCB, LDHA/B and of additional proteins absent in our MS/MS data but known to play important roles in metabolism: PDK, MCT1/4, GLUT1, HK2 (Figure 6).

PC overexpression was specific to cancer thyrocytes (Figure 6a), as were two other overexpressed enzymes linked to the metabolism of oxaloacetate: phosphoenolpyruvate carboxykinase 2 (PCK2) (Figure 6a) and pyruvate dehydrogenase (PDH) (Figure 6c), the latter being responsible for pyruvate decarboxylation into acetyl-CoA, an allosteric activator of PC. These data suggest that anaplerosis occurs in PTC with PC mediating oxaloacetate entrance into the TCA cycle. Interestingly, pyruvate dehydrogenase kinase (PDK) which inhibits PDH and is described in many cancers as overexpressed, was not deregulated in PTC (Figure 6c). Protein levels for PDHα1 and PDK were also analyzed by Western blotting: PDHα1 was strongly upregulated in 2/8 samples and weakly upregulated in 4/8 samples, while PDK levels remained constant in most of the samples (data not shown). In addition, GLS was also specifically increased in tumor cells, suggesting the existence of the other major anaplerotic reaction (Figure 6a). Two enzymes implicated in β-oxidation of lipids leading to acetyl-CoA production were analyzed: 3-5, 2-4, dienoyl-CoA isomerase (ECH1) and propionyl-CoA

carboxylase B subunit (PCCB). Both were also specifically upregulated in the cancer cells, suggesting an increased production of acetyl-CoA in these cells (Figure 6a).

LDH showed increased expression in cancer cells and in CAFs, and this was observed for LDHA and LDHB (Figure 6b). Since LDH is a tetramer composed of two different subunits (LDH-M and LDH-H, respectively encoded by the LDHA and LDHB genes) present in variable proportions, these results could be explained by the existence of mixed isoforms of LDH, all recognized by the specific anti-LDHA and anti-LDHB antibodies. The monocarboxylate transporter MCT1, mediating the uptake of lactate, was only overexpressed in the cancer cells while MCT4, triggering the export of lactate, was found in tumor cells and was also weakly expressed in CAFs in some areas (Figure 6b). Finally, we analyzed the expression of HK2 and of the glucose transporter GLUT1. As depicted in Figure 6b, both enzymes were specifically overexpressed in the thyroid cancer cells. HK2 showed a heterogeneous expression across the entire tumor with some tumor cells expressing higher levels of this enzyme.

DISCUSSION:

Scientific domains in cancer research are clean and easily understandable as long as they are kept distinct. However, as soon as concepts and findings in one domain are extended to another, difficulties and discrepancies appear. Whereas the cause and initial genetic mechanism of a particular tumor may be well defined, its phenotype and even genotype evolve in space and time, resulting in spatial and temporal heterogeneities. Experimentally, studies on whole tissues (e.g. omics studies) ignore the morphological and metabolic heterogeneity of the tumor. On the other hand, clean experimental studies *in vitro* (e.g. cancer cells, cell lines) and *in vivo* ignore tissue complexity (30).

With regard to cancer metabolism, much has been learned about the versatility of *in vitro* models depending on the culturing conditions, for instance the existence of both the Warburg

and the reverse Warburg effects, the alternative use of substrates depending on their availability, the roles of lactate and H^+ as metabolites and signals (31). On the other hand, the description of cancers *in vivo* is based mostly on observations at one point in time ("snapshots"). It is therefore interesting to investigate which situation exists *in vivo* in human cancers. For this, global measurements (genetics, expressions…) should be complemented by methods allowing to define spatial and time distributions of properties. In this study, we have tried to integrate some fundamental experimental concepts on tumor energetic metabolism, in order to define the spatial characteristics of metabolism, Warburg effect, and anaplerosis of the well-defined, most frequent, human thyroid cancer: the PTC. This could bring a few conceptual bridges between experimental and physiopathological concepts.

Since decades, the hypothesis of Otto Warburg orientated cancer researches to better understand how tumors work and to find new treatments. According to the Warburg effect, tumors have an increased glycolysis and a drastically reduced oxidative mitochondrial activity, which led to develop therapies specifically targeting the glycolytic pathway (32, 33). However several studies demonstrated that the TCA cycle is still functional in some tumors and produces catabolic precursors for their proliferative needs (6). In this study, we show that PTC have a very active TCA cycle, in opposition to the Warburg model, and this activity is not mutually exclusive with glycolysis since both metabolic pathways are present.

As energetic metabolism in PTC is poorly characterized, we decided to investigate the metabolic alterations in these tumors. A proteomic analysis of 5 PTC revealed the upregulation of a high number of proteins involved in metabolism, which were further characterized. Although the number of samples analyzed is too low to draw definite conclusions, these deregulations seem to be amplified according to tumor stage, suggesting a correlation between increased energetic metabolism and tumor aggressiveness. Accordingly, Nahm et al showed

that the expression of glycolysis-related proteins was correlated with poorer prognosis (17). Pyruvate carboxylase appeared to be overexpressed at both mRNA and protein levels, a new finding in the field. This enzyme that allows pyruvate to be carboxylated into oxaloacetate, funneled in the TCA cycle, was only recently described as deregulated in lung and breast cancers (34, 35). This suggests that pyruvate is not systematically transformed into lactate according to the Warburg effect, but could be an essential resource to maintain the oxidative mitochondrial metabolism. We first defined the functional role of PC in thyroid cell lines. Two commonly used thyroid cancer cell lines, TPC1 and 8505C (23, 25), and HTori-3 cells, non-tumorigenic SV40-immortalized human thyrocytes (24) were used for this purpose. Although TPC1 and 8505C cells respectively derive from a PTC and an ATC, these cell lines have evolved into a common, dedifferentiated phenotype (23, 25). Thus, TPC1 and 8505C cells were not chosen as a relevant model for the corresponding *in vivo* tumor, but rather as thyroid cancer experimental *in vitro* models. Both cell types showed decreased proliferation, migration, invasion and mitochondrial respiration rates following PC knockdown, suggesting a role of PC in generating energy and metabolic precursors through the pyruvate conversion into oxaloacetate and its consumption by the TCA cycle. No changes were observed in the proliferation and invasion rates in HTori-3 cells following PC knockdown, but their migration rate and their oxygen consumption were reduced. The non-tumorigenic character and the non-cancer origin of HTori-3 cells might explain these differences.

Cellular heterogeneity is an emerging concept in interpreting cancer biology, and PTC are indeed heterogeneous tumors, containing thyroid cells, stromal cells such as cancer-associated fibroblasts, lymphocytes and endothelial cells. To further explore the increased oxidative mitochondrial metabolism in PTC, and to analyze the contribution of the different cell types, we investigated the cellular distribution of several metabolic proteins in the cancer and in the

stromal cells by IHC. PC, PCK2 and PDHα1, three enzymes related to the metabolism of oxaloacetate, were specifically overexpressed in cancer thyrocytes, whereas the expression of PDK, an inhibitor of PDH, remained unchanged. PC and PDH, by producing respectively oxaloacetate and acetyl-CoA, itself an allosteric activator of PC, contribute to replenish the TCA cycle. PCK2, the mitochondrial isoform of PCK, although well-known for its role in gluconeogenesis, underlines the importance of TCA cycle in absence of glucose (36). The overexpression of PDH, observed in 75% of the samples, and the absence of deregulation of PDK are in opposition to what has been described for other cancers, such as non-small cell lung carcinomas where the repression of the PDH/PDK pathway has been related with aerobic glycolysis/Warburg effect (37). Taken together, our data support the presence of an actively functioning TCA cycle in PTC, involving pyruvate metabolism. In addition, they also suggest that acetyl-CoA can be produced from lipid degradation since several enzymes involved in this pathway showed an increased expression, as measured by MS/MS. Among them, the specific overexpression in cancer cells of ECH1 and PCCB was confirmed by IHC. This is in agreement with other studies reporting a role of lipid degradation in cancers, such as in the triple negative breast cancer, following stress conditions (38, 39).

The other important anaplerotic reaction able to replenish the TCA cycle, i.e. glutaminolysis, also appears to sustain the energetic metabolism in PTC. Indeed, an overexpression of GLS was observed in the cancerous cells of the PTC and glutamine was identified as an essential nutrient in thyroid cell lines tested for oxidative respiration. Inhibiting glutaminase by BPTES highlighted the existence of a compensatory relationship between GLS and PC, already described for glioblastoma cells in culture and in xenografts (12), in addition to the anaplerotic role of GLS.

All the enzymes involved in oxidative metabolism that were studied were specifically overexpressed in thyroid cancer cells. Cancer-associated fibroblasts have been described in other cancers such as breast and brain cancers to feed cancerous cells by producing lactate into the tumor microenvironment (10, 40). Our data show that the LDH enzymes are present in cancerous cells and in CAFs, but do not allow to definitively conclude on the metabolism of lactate. Regarding the lactate transporters, MCT1 (uptake of lactate) is overexpressed in the tumor cells while MCT4 (export of lactate) is present in tumor cells but also weakly expressed in CAFs in some areas. This confirms other studies on thyroid cancer (22), and suggests that lactate is released from cancerous cells, and from CAFs in some areas of the tissue, and is taken up by other cancerous cells, allowing production of ATP through mitochondrial oxidative phosphorylation. It supports the metabolic model of the reverse Warburg effect between cancerous cells and CAFs as well as the existence of a metabolic symbiosis between cancer cells that are not equal with regard to oxygen availability (41). Finally, we investigated the origin of pyruvate, which could derive from glucose but also from lactate. Our proteomic data revealed an overall upregulation of the glycolytic enzymes in the 5 PTC analyzed. We performed IHC with GLUT1 and HK2 antibodies, and we observed that both enzymes were specifically overexpressed in tumor cells, confirming a previous report (17). The overexpression of GLUT1 is consistent with the observation that, in differentiated thyroid carcinomas, glucose uptake of $BRAF^{V600E}$ positive tumors was higher than that of BRAF wild type tumors (16). In addition, the overall survival of patients with high GLUT1 expression is reduced (17). Altogether, our results suggest that, in PTC, glucose would be distributed between the TCA cycle and the production of lactate, as it was reported in KRAS-mutated non-small cell lung cancers (NSCLC) (20), in glioblastomas (42) and in bladder cancer (43).

In conclusion, pyruvate carboxylase is a key enzyme in thyroid cancer cells, at the intersection between glycolysis and the TCA cycle, playing an important role in anaplerosis. The distribution of other overexpressed enzymes showed that the TCA cycle is very active in tumor cells. However, our results give only a snapshot of the Warburg effect, metabolism, and anaplerosis in PTC at the time of tissue collection. They do not consider the evolution of the described temporal heterogeneity. For this, further *in vivo* studies, e.g. a ^{13}C-tracer analysis with labeled glucose and lactate, could provide information about carbon trafficking inside the tumors (44). Hypoxia should also be investigated in PTC to identify areas with distinct metabolic adaptations. Exploring the expression pattern of the different metabolic proteins comparing central and peripheral tumor areas might also bring interesting information regarding tumor heterogeneity. Such knowledge could give a basis for the rational use of new therapeutic tools targeting tumor metabolism (14, 33). However, this concept implies that all the cells exhibit the same pattern at the same time, which in the case of metabolism, is not true (30, 45). Moreover, cancer cells are able to adapt to changing conditions by shifting from one metabolic pattern to another.

ACKNOWLEDGMENTS

This study was supported by grants from the Fonds de la Recherche Scientifique FNRS-FRSM, Fonds J-P Naets, Fondation Roi Baudouin.

CM, JD and ASt conceived the experiments; ASt and CC carried out the experiments; CM, ASt interpreted the results and wrote the manuscript; GD, CC, OF helped with data analysis; GA collected patient samples; ASp, LC and DL collected and reviewed the histopathological slices of the thyroid cancers; RW performed the MS/MS analysis.

The authors thank Chantal Degraef, Claude Massart, Bernadette Bournonville for the excellent technical support.

AUTHOR DISCLOSURE STATEMENT

Protocols have been approved and consent by the Ethics Committee of the J. Bordet Institute (protocol number: 1978), in accordance with the Declaration of Helsinki.

No competing financial interests exist.

REFERENCES

1. DeBerardinis RJ, Chandel NS 2016 Fundamentals of cancer metabolism. Sci Adv **2**:e1600200–e1600200.
2. Hanahan D, Weinberg RA 2011 Hallmarks of cancer: The next generation. Cell **144**:646–674.
3. Cairns R a, Harris I, McCracken S, Mak TW 2011 Cancer cell metabolism. Cold Spring Harb Symp Quant Biol **76**:299–311.
4. Warburg O, Wind F, Negelein E 1927 I . Killing-Off of Tumor Cells in Vitro . J Gen Physiol **8**:519–530.
5. Ferreira LMR, Hebrant A, Dumont JE 2012 Metabolic reprogramming of the tumor. Oncogene **31**:3999–4011.
6. Ward PS, Thompson CB 2012 Metabolic Reprogramming: A Cancer Hallmark Even Warburg Did Not Anticipate. Cancer Cell **21**:297–308.
7. Orimo A, Weinberg RA 2006 Stromal Fibroblasts in Cancer: A Novel Tumor-Promoting Cell Type. Cell Cycle **5**:1597–1601.

8. Pietras K, Östman A 2010 Hallmarks of cancer: Interactions with the tumor stroma. Exp Cell Res **316**:1324–1331.

9. Fiaschi T, Giannoni E, Taddei ML, Cirri P, Marini A, Pintus G, Nativi C, Richichi B, Scozzafava A, Carta F, Torre E, Supuran CT, Chiarugi P 2013 Carbonic anhydrase IX from cancer-associated fibroblasts drives epithelial-mesenchymal transition in prostate carcinoma cells. Cell Cycle **12**:1791–1801.

10. Pavlides S, Whitaker-Menezes D, Castello-Cros R, Flomenberg N, Witkiewicz AK, Frank PG, Casimiro MC, Wang C, Fortina P, Addya S, Pestell RG, Martinez-Outschoorn UE, Sotgia F, Lisanti MP 2009 The reverse Warburg effect: Aerobic glycolysis in cancer associated fibroblasts and the tumor stroma. Cell Cycle **8**:3984–4001.

11. Whitaker-Menezes D, Martinez-Outschoorn UE, Lin Z, Ertel A, Flomenberg N, Witkiewicz AK, Birbe RC, Howell A, Pavlides S, Gandara R, Pestell RG, Sotgia F, Philp NJ, Lisanti MP 2011 Evidence for a stromal-epithelial "lactate shuttle" in human tumors: MCT4 is a marker of oxidative stress in cancer-associated fibroblasts. Cell Cycle **10**:1772–1783.

12. Cheng T, Sudderth J, Yang C, Mullen AR, Jin ES, Mates JM, DeBerardinis RJ 2011 Pyruvate carboxylase is required for glutamine-independent growth of tumor cells. Proc Natl Acad Sci **108**:8674–8679.

13. Pérez-Escuredo J, Dadhich RK, Dhup S, Cacace A, Van Hée VF, De Saedeleer CJ, Sboarina M, Rodriguez F, Fontenille M-J, Brisson L, Porporato PE, Sonveaux P 2016 Lactate promotes glutamine uptake and metabolism in oxidative cancer cells. Cell Cycle **15**:72–83.

14. Doherty J, Cleveland J 2013 Targeting lactate metabolism for cancer therapeutics. J Clin Invest **123**:3685–3692.

15. Kim HM, Lee YK, Koo JS 2016 Expression of glutamine metabolism-related proteins in thyroid cancer. Oncotarget **7**:53628–53641.

16. Nagarajah J, Ho AL, Tuttle RM, Weber WA, Grewal RK 2015 Correlation of BRAFV600E Mutation and Glucose Metabolism in Thyroid Cancer Patients: An 18F-FDG PET Study. J Nucl Med **56**:662–667.

17. Nahm JH, Kim HM, Koo JS 2017 Glycolysis-related protein expression in thyroid cancer. Tumor Biol **39**:101042831769592.

18. Yoon M, Jung SJ, Kim TH, Ha TK, Urm S-H, Park JS, Lee SM, Bae SK 2016 Relationships between transporter expression and the status of BRAF V600E mutation and F-18 FDG uptake in papillary thyroid carcinomas. Endocr Res **41**:64–69.

19. Christen S, Lorendeau D, Schmieder R, Broekaert D, Metzger K, Veys K, Elia I, Buescher JM, Orth MF, Davidson SM, Grünewald TGP, De Bock K, Fendt SM 2016 Breast Cancer-Derived Lung Metastases Show Increased Pyruvate Carboxylase-Dependent Anaplerosis. Cell Rep **17**:837–848.

20. Davidson SM, Papagiannakopoulos T, Olenchock BA, Heyman JE, Keibler MA, Luengo A, Bauer MR, Jha AK, O'Brien JP, Pierce KA, Gui DY, Sullivan LB, Wasylenko TM, Subbaraj L, Chin CR, Stephanopolous G, Mott BT, Jacks T, Clish CB, Van Der Heiden MG 2016 Environment impacts the metabolic dependencies of ras-driven non-small cell lung cancer. Cell Metab **23**:517–528.

21. Tarabichi M, Antoniou A, Le Pennec S, Gacquer D, de Saint Aubain N, Craciun L, Cielen T, Laios I, Larsimont D, Andry G, Dumont JE, Maenhaut C, Detours V 2017 Distinctive desmoplastic 3D morphology associated with BRAF V600E in papillary thyroid cancers.

22. Gill KS, Tassone P, Hamilton J, Hjelm N, Luginbuhl A, Cognetti D, Tuluc M, Martinez-Outschoorn U, Johnson JM, Curry JM 2016 Thyroid Cancer Metabolism: A

Review. J Thyroid Disord Ther **5**.

23. Saiselet M, Floor S, Tarabichi M, Dom G, Hébrant A 2012 Thyroid cancer cell lines : an overview. Front Endocrinol **3**:1–9.

24. Lemoine NR, Mayall ES, Jones T, Sheer D, Mcdermid S 1989 Characterisation of human thyroid epithelial cells immortalised in vitro by simian virus 40 DNA transfection. Br J Cancer **2**:897–903.

25. Staveren WCG Van, Solı DW, Delys L, Duprez L, Andry G, Franc B, Thomas G, Dumont JE, Detours V, Maenhaut C 2007 Human Thyroid Tumor Cell Lines Derived from Different Tumor Types Present a Common Dedifferentiated Phenotype. Cancer Res **67**: 8113–8121.

26. Schweppe RE, Klopper JP, Korch C, Pugazhenthi U, Benezra M, Knauf JA, Fagin JA, Marlow LA, Copland JA, Smallridge RC, Haugen BR 2008 Deoxyribonucleic Acid Profiling Analysis of Cross-Contamination Resulting in Cell Line Redundancy and Misidentification. J Clin Endocrinol Metab **93**:4331–4341.

27. Delys L, Detours V, Franc B, Thomas G, Bogdanova T, Tronko M, Libert F, Dumont JE, Maenhaut C 2007 Gene expression and the biological phenotype of papillary thyroid carcinomas. Oncogene **26**:7894–7903.

28. Tian Q, Stepaniants SB, Mao M, Weng L, Feetham MC, Doyle MJ, Yi EC, Dai H, Thorsson V, Eng J, Goodlett D, Berger JP, Gunter B, Linseley PS, Stoughton RB, Aebersold R, Collins SJ, Hanlon WA, Hood LE 2004 Integrated genomic and proteomic analyses of gene expression in Mammalian cells. Mol Cell Proteomics **3**:960–9.

29. Hébrant A, Dom G, Dewaele M, Andry G, Trésallet C, Leteurtre E, Dumont JE, Maenhaut C 2012 mRNA expression in papillary and anaplastic thyroid carcinoma: molecular anatomy of a killing switch. PLoS One **7**:e37807.

30. Strickaert A, Saiselet M, Dom G, De Deken X, Dumont JE, Feron O, Sonveaux P, Maenhaut C 2016 Cancer heterogeneity is not compatible with one unique cancer cell metabolic map. Oncogene 1–6.

31. Corbet C, Feron O 2017 Tumour acidosis: from the passenger to the driver's seat. Nat Rev Cancer **17**:577–593.

32. Ganapathy-Kanniappan S, Geschwind J-FH 2013 Tumor glycolysis as a target for cancer therapy: progress and prospects. Mol Cancer **12**:152.

33. Porporato PE, Dhup S, Dadhich RK, Copetti T, Sonveaux P 2011 Anticancer targets in the glycolytic metabolism of tumors: A comprehensive review. Front Pharmacol **AUG**:1–18.

34. Sellers K, Fox MP, Ii MB, Slone SP, Higashi RM, Miller DM, Wang Y, Yan J, Yuneva MO, Deshpande R, Lane AN, Fan TW 2015 Pyruvate carboxylase is critical for non – small-cell lung cancer proliferation. J Clin Invest **125**:687–698.

35. Phannasil P, Thuwajit C, Warnnissorn M, Wallace JC, MacDonald MJ, Jitrapakdee S 2015 Pyruvate carboxylase is up-regulated in breast cancer and essential to support growth and invasion of MDA-MB-231 cells. PLoS One **10**:1–20.

36. Vincent EE, Sergushichev A, Griss T, Gingras MC, Samborska B, Ntimbane T, Coelho PP, Blagih J, Raissi TC, Choinière L, Bridon G, Loginicheva E, Flynn BR, Thomas EC, Tavaré JM, Avizonis D, Pause A, Elder DJE, Artyomov MN, Jones RG 2015 Mitochondrial Phosphoenolpyruvate Carboxykinase Regulates Metabolic Adaptation and Enables Glucose-Independent Tumor Growth. Mol Cell **60**:195–207.

37. Chen JQ, Russo J 2012 Dysregulation of glucose transport, glycolysis, TCA cycle and glutaminolysis by oncogenes and tumor suppressors in cancer cells. Biochim Biophys Acta - Rev Cancer **1826**:370–384.

38. Röhrig F, Schulze A 2016 The multifaceted roles of fatty acid synthesis in cancer. Nat

Rev Cancer **16**:732–749.

39. Park JH, Vithayathil S, Kumar S, Sung P-L, Dobrolecki LE, Putluri V, Bhat VB, Bhowmik SK, Gupta V, Arora K, Wu D, Tsouko E, Zhang Y, Maity S, Taraka R, Graham BH, Frigo DE, Coarfa C, Yotnda P, Sreekumar A, Lewis MT, Creighton CJ, Wong LC, Kaipparettu BA 2016 Fatty Acid Oxidation-Driven Src Links Mitochondrial Energy Reprogramming and Regulation of Oncogenic Properties in Triple Negative Breast Cancer. Cell Rep **14**:2154–2165.

40. Pérez-Escuredo J, Van Hée VF, Sboarina M, Falces J, Payen VL, Pellerin L, Sonveaux P 2016 Monocarboxylate transporters in the brain and in cancer. Biochim Biophys Acta.

41. Feron O 2009 Pyruvate into lactate and back: From the Warburg effect to symbiotic energy fuel exchange in cancer cells. Radiother Oncol **92**:329–333.

42. Maher EA, Marin-Valencia I, Bachoo RM, Mashimo T, Raisanen J, Hatanpaa KJ, Jindal A, Jeffrey FM, Choi C, Madden C, Mathews D, Pascual JM, Mickey BE, Malloy CR, DeBerardinis RJ 2012 Metabolism of [U-13C]glucose in human brain tumors in vivo. NMR Biomed **25**:1234–1244.

43. Afonso J, Santos LL, Morais A, Amaro T, Longatto-Filho A, Baltazar F 2016 Metabolic coupling in urothelial bladder cancer compartments and its correlation to tumor aggressiveness. Cell Cycle **15**:368–380.

44. Hensley CT, Faubert B, Yuan Q, Lev-Cohain N, Jin E, Kim J, Jiang L, Ko B, Skelton R, Loudat L, Wodzak M, Klimko C, McMillan E, Butt Y, Ni M, Oliver D, Torrealba J, Malloy CR, Kernstine K, Lenkinski RE, DeBerardinis RJ 2016 Metabolic Heterogeneity in Human Lung Tumors. Cell **164**:681–694.

45. Swanton C 2012 Intratumour Heterogeneity : Evolution through Space and Time. Cancer Res **72**:4875–4882.

FIGURE LEGENDS

Figure 1: **Protein expression levels of metabolic enzymes or proteins measured by MS/MS analysis, and presented in log2 of expression ratios (tumor/normal)**. DB number = accession number in Uniprot database. Cutoff of the expression ratios in log2 is 1; (red: expression level ≥ 1; green: expression level ≤ -1).

Figure 2: Heatmap of mRNA expression levels of metabolic proteins. Expression levels were obtained by Affymetrix microarrays and are presented in log2 of expression ratios (tumor/normal). Genes were grouped by metabolic pathways: glycolysis, TCA cycle et "others". PTCa-e were the 5 PTC analyzed by MS/MS spectrometry.

Figure 3: Pyruvate carboxylase expression in PTC. (a,b) : Upregulation of PC mRNA was measured by qRT-PCR, and the results are presented as log2 of expression ratios (a: tumor versus normal adjacent tissue; b: tumor versus a pool of 22 normal tissues). The expressions were normalized with the housekeeping genes NEDD8 et TTC1. (c) The upregulation of PC was validated at the protein level by Western blotting (N: normal; T: tumor).

Figure 4: PC knockdown following siRNA transfection and functional effects in thyroid cell lines. Transfection of siRNA against PC (siPC) was performed in 3 thyroid cell lines (TPC1, 8505C et HTori). Cell lines were also transfected with a negative control siRNA (siCTRL) or not transfected (NT). PC expression was measured (a) at the mRNA level by qRT-PCR after 48 hours in TPC1 cells and (b) at the protein level by Western blotting after 72 hours in the three cell lines (n=5). The mRNA expressions are represented with the mean ± SD, and the t-test showed a significant difference between transfected conditions (siCTRL vs siPC);

***: p-value < 0.001. (c) Cell lines were labelled with EdU 72 after siRNA transfection and the percentage of EdU positive cells among 10 000 cells was analyzed by flow cytometry (N=4). Results are represented with mean ± SD, and a student paired t-test showed a significant difference between transfected conditions (siCTRL vs siPC); *: p-value = 0,0247; **: p-value = 0,017; ns: not significant. (d)(e) Cells were seeded in migration or invasion chambers. FBS was used as chemoattractant. The cells were counted after (d) migration through the porous membrane, (e) invasion through the matrigel membrane (N=3). Results are represented with mean ± SD, and a t-test showed a significant difference between transfection conditions (siCTRL vs siPC) for TPC1 and 8505C cells; *: p-value < 0.05; **: p-value < 0.001; ns: not significant.

Figure 5: Oxygen consumption rates measurements following PC knockdown. TPC1, HTori and 8505C cells were transfected with siPC or siCTRL 72h before OCR measurements, which were taken before and after substrate addition. Substrates: Glc: glucose, Lac: lactate, Pyr: pyruvate, Gln: glutamine. BPTES: glutaminase inhibitor. (a) ΔOCR data for one representative experiment of 2 independent ones (2 biological replicates) and 6 measurements by experiment (6 technical replicates). (b) OCR over time data for one representative experiment with 6 measurements (6 technical replicates) for each time point before and after the addition of pyruvate.

Figure 6: Expression of different metabolic enzymes and transporters in PTC and their normal adjacent tissues (N). (a)(b) Immunostainings were performed on paraffin sections with antibodies against the following proteins: PC, PCK2, GLS, ECH1, PCCB, LDHA, LDHB, MCT1, MCT4, HK2, GLUT1, PDHα1, and PDK (N=4). A negative control (no primary

antibody) has been performed to confirm the specificity of each antibody. ~~(c) Expression levels of PDHα1 and PDK were measured by Western blotting. N: normal, T: tumor.~~

SUPPLEMENTARY DATA

Figure S: DNA profiling by STR analysis of the HTori-3 cell line.

Table S1: Patient information, clinical data, and presence of BRAF-mutation for the 5 PTC analyzed by MS/MS. W: woman, M: man, TNM: tumor lymph nodes metastasis, mut: mutation

Table S2: Identified proteins by MS/MS with a more than 2 fold deregulated expression in the 5 PTC compared to normal tissues. Green: log2 ratios of underexpressed proteins in tumors; Red: log2 ratios of overexpressed proteins in tumors.

	Protein	Name	DB number	PTC-a	PTC-b	PTC-c	PTC-d	PTC-e
GLYCOLYSIS	HK1	Hexokinase 1	E7ENR4	1,2	1,7	2,8	0,8	-0,1
	GPI	Glucose-6-phosphate isomerase	B4DG39	0,7	0,2	1,7	-0,7	1,3
	PFKP	Phosphofructokinase, platelet	Q5VSR7	-2,2	1,5	3,5	1,1	0,4
	ALDOA	Fructose-bisphosphate aldolase	B7Z3K9	0,7	1,1	1,0	0,8	0,6
	TPI	Triosephosphate isomerase	Q53HE2	0,9	1,6	2,4	1,8	0,8
	GAPDH	Glyceraldehyde-3-phosphate dehydrogenase	E7EUT4	1,1	1,6	1,7	1,3	1,2
	PGK1	Phosphoglycerate kinase 1	A8K4W6	0,5	1,7	-2,1	0,9	-0,3
	PGM	Phosphoglycerate mutase	Q53G35	-0,1	-0,8	1,0	0,5	3,3
	ENO2	Enolase 2	Q6FHV6	1,0	1,1	1,9	1,4	0,0
	PKM2	Pyruvate kinase	B4DUU6	1,3	1,6	1,6	1,3	-0,7
TCA CYCLE	PC	Pyruvate carboxylase	E9PS68	3,0	3,7	3,2	2,7	2,2
	PDHA1	Pyruvate dehydrogenase subunit A1	A5YVE9	3,7	3,0	1,8	1,1	1,6
	PDHB	Pyruvate dehydrogenase subunit B	B4DDD7	1,0	0,2	2,4	0,9	1,5
	DLAT	Dihydrolipoamide S-acetyltransferase	Q86YI5	0,8	2,8	6,1	1,4	1,3
	PDHX	Pyruvate dehydrogenase complex, component X	B2R673	0,3	-0,1	2,7	1,2	3,3
	PCK2	Pyruvate carboxykinase	Q6IB91	1,1	5,4	2,6	1,2	0,8
	CS	Citrate synthase	B4DJV2	2,0	2,4	2,3	2,0	1,2
	ACO2	Aconitase 2	A2A274	0,5	4,0	2,0	0,3	1,7
	IDH2	Isocitrate dehydrogenase 2	Q53GL5	1,3	2,4	1,7	0,2	2,5
	FH	Fumarate hydratase	B1ANK7	1,9	0,6	3,3	2,1	2,2
	SUCLG2	Succinate-CoA ligase subunit beta	C9JVT2	2,1	5,3	4,8	1,9	2,0
	SDHB	Succinate dehydrogenase complex subunit B	Q0QEY7	1,0	2,2	4,0	6,7	1,7
	MDH2	Malate dehydrogenase 2	Q6FHZ0	-1,9	-0,1	2,0	0,5	0,0
OTHERS	ME	Malic enzyme	B2R8J2	-0,1	2,0	4,0	4,9	2,8
	MDH1	Malate dehydrogenase 1	F5H098	0,8	0,7	1,1	0,2	1,0
	CTP	Mitochondrial citrate transport protein	Q6LAP8	1,0	3,1	2,3	2,1	4,0
	PCCA	Propionyl Coenzyme A carboxylase, alpha	B2RDE0	1,6	1,1	2,3	1,7	3,2
	PCCB	Propionyl Coenzyme A carboxylase, bêta	E7EX59	0,0	3,5	4,3	-0,9	3,2
	ECH1	3,5-delta 2,4-dienoyl-CoA isomerase, mitochondrial	B4DVS4	5,4	2,9	1,8	1,1	5,2
	LDHA	L-lactate dehydrogenase A	B7Z5E3	1,4	1,4	1,7	0,6	1,2
	LDHB	L-lactate dehydrogenase B	Q5U077	1,0	-0,2	1,3	0,4	1,2
	GLS	Glutaminase	A8K132	-1,9	1,9	5,8	3,1	4,3

Figure 1: Protein expression levels of metabolic enzymes or proteins measured by MS/MS analysis, and presented in log2 of expression ratios (tumor/normal). DB number = accession number in Uniprot database. Cutoff of the expression ratios in log2 is 1; (red: expression level ≥ 1; green: expression level ≤ -1).

227x180mm (300 x 300 DPI)

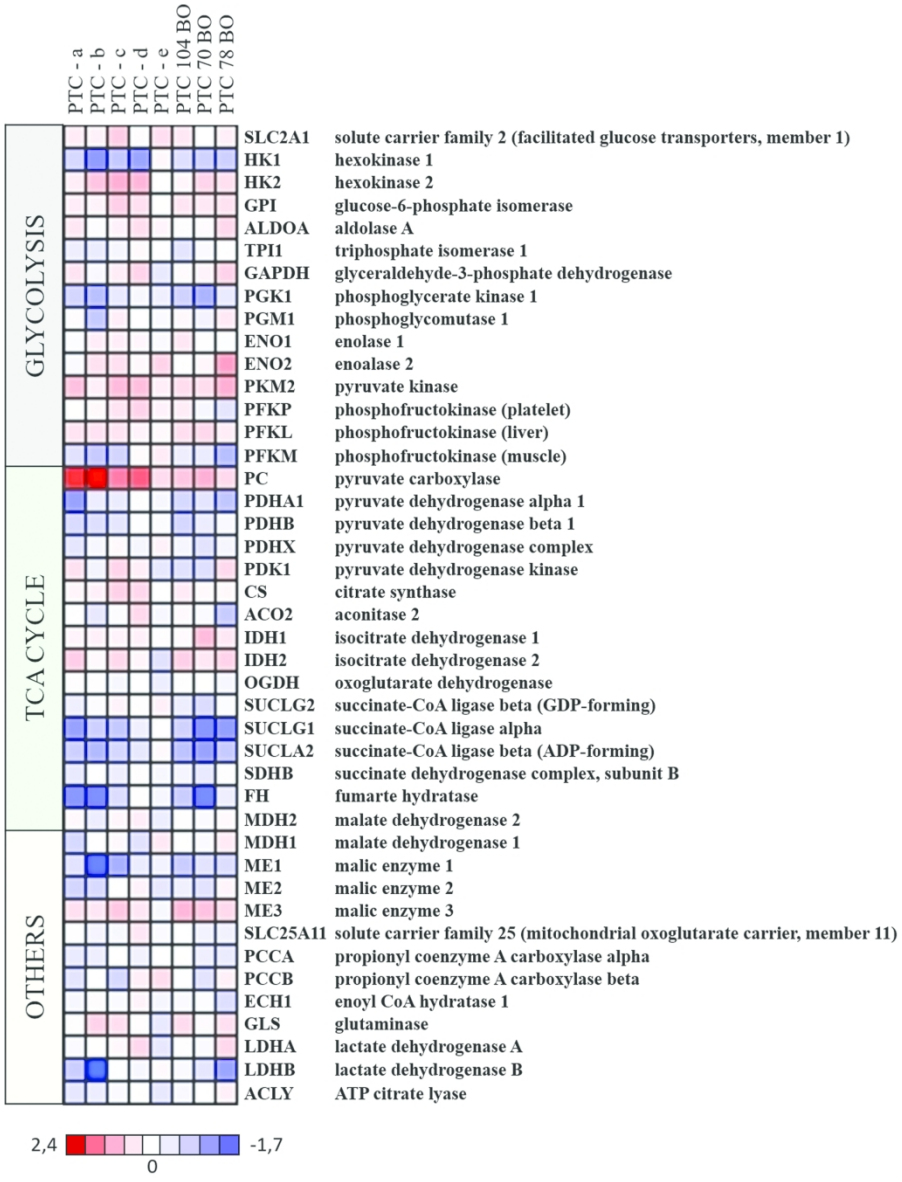

Figure 2: Heatmap of mRNA expression levels of metabolic proteins. Expression levels were obtained by Affymetrix microarrays and are presented in log2 of expression ratios (tumor/normal). Genes were grouped by metabolic pathways: glycolysis, TCA cycle et "others". PTCa-e were the 5 PTC analyzed by MS/MS spectrometry.

225x280mm (300 x 300 DPI)

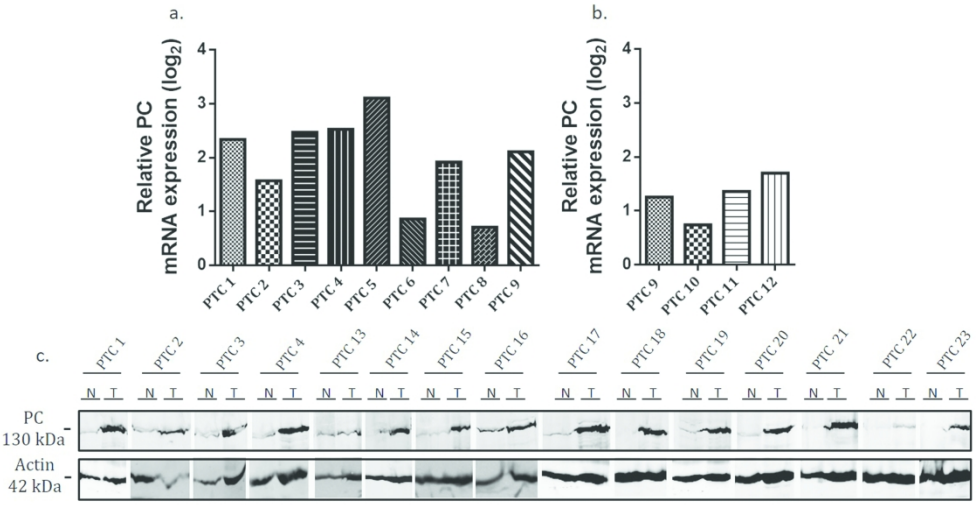

Figure 3: Pyruvate carboxylase expression in PTC. (a,b) : Upregulation of PC mRNA was measured by qRT-PCR, and the results are presented as log2 of expression ratios (a: tumor versus normal adjacent tissue; b: tumor versus a pool of 22 normal tissues). The expressions were normalized with the housekeeping genes NEDD8 et TTC1. (c) The upregulation of PC was validated at the protein level by Western blotting (N: normal; T: tumor).

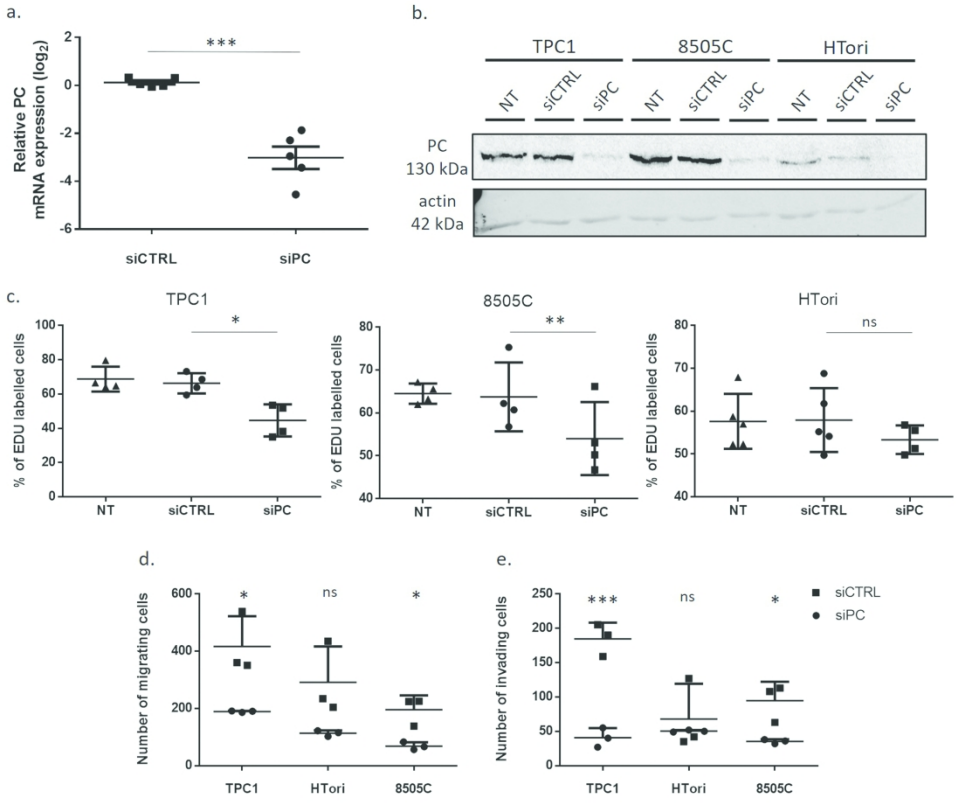

Figure 4: PC knockdown following siRNA transfection and functional effects in thyroid cell lines. Transfection of siRNA against PC (siPC) was performed in 3 thyroid cell lines (TPC1, 8505C et HTori). Cell lines were also transfected with a negative control siRNA (siCTRL) or not transfected (NT). PC expression was measured (a) at the mRNA level by qRT-PCR after 48 hours in TPC1 cells and (b) at the protein level by Western blotting after 72 hours in the three cell lines (n=5). The mRNA expressions are represented with the mean ± SD, and the t-test showed a significant difference between transfected conditions (siCTRL vs siPC); ***: p-value < 0.001. (c) Cell lines were labelled with EdU 72 after siRNA transfection and the percentage of EdU positive cells among 10 000 cells was analyzed by flow cytometry (N=4). Results are represented with mean ± SD, and a student paired t-test showed a significant difference between transfected conditions (siCTRL vs siPC); *: p-value = 0,0247; **: p-value = 0,017; ns: not significant. (d)(e) Cells were seeded in migration or invasion chambers. FBS was used as chemoattractant. The cells were counted after (d) migration through the porous membrane, (e) invasion through the matrigel membrane (N=3). Results are represented with mean ± SD, and a t-test showed a significant difference between transfection conditions (siCTRL vs siPC) for TPC1 and 8505C cells; *: p-value < 0.05; **: p-value < 0.001; ns: not significant.

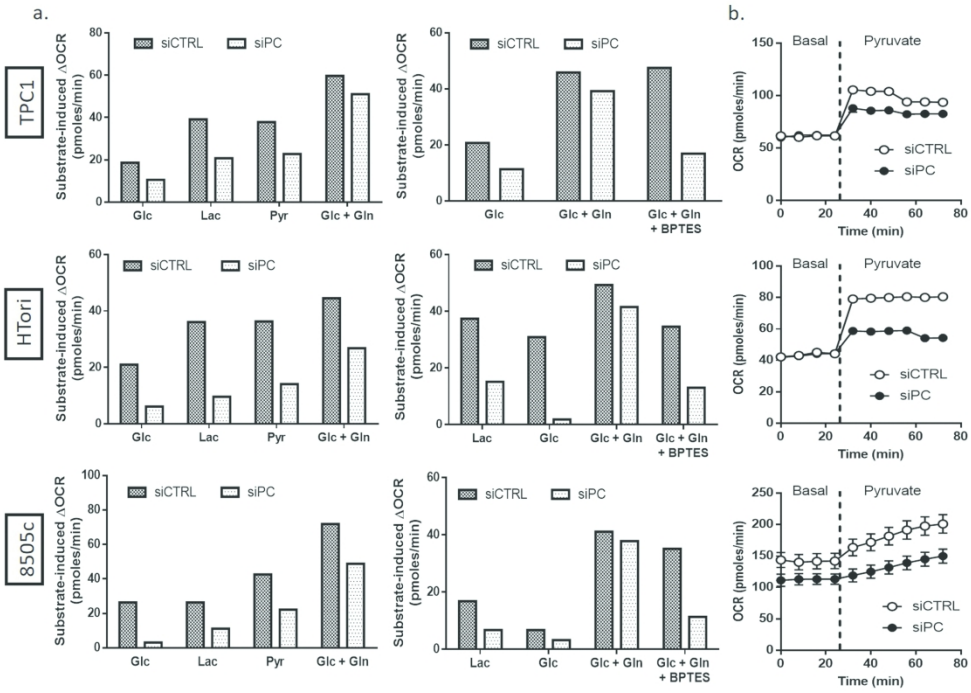

Figure 5: Oxygen consumption rates measurements following PC knockdown. TPC1, HTori and 8505C cells were transfected with siPC or siCTRL 72h before OCR measurements, which were taken before and after substrate addition. Substrates: Glc: glucose, Lac: lactate, Pyr: pyruvate, Gln: glutamine. BPTES: glutaminase inhibitor. (a) ΔOCR data for one representative experiment of 2 independent ones (2 biological replicates) and 6 measurements by experiment (6 technical replicates). (b) OCR over time data for one representative experiment with 6 measurements (6 technical replicates) for each time point before and after the addition of pyruvate.

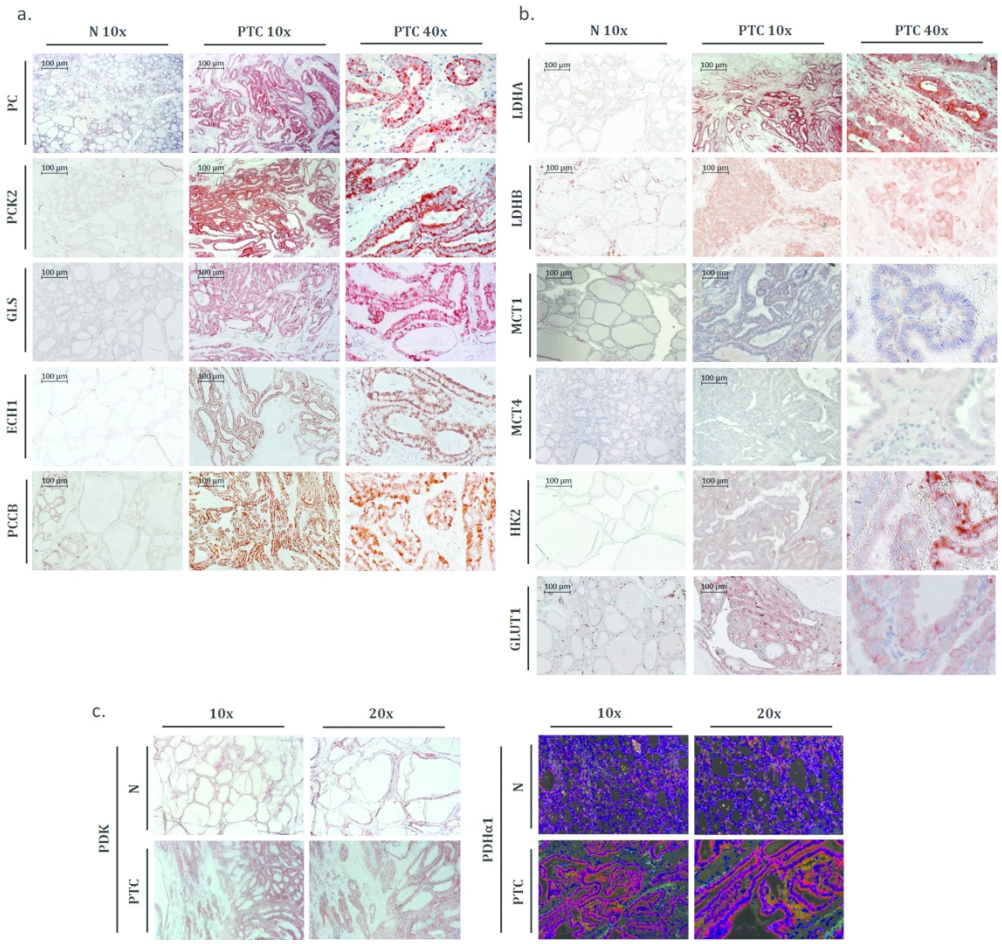

Figure 6: Expression of different metabolic enzymes and transporters in PTC and their normal adjacent tissues (N). (a)(b) Immunostainings were performed on paraffin sections with antibodies against the following proteins: PC, PCK2, GLS, ECH1, PCCB, LDHA, LDHB, MCT1, MCT4, HK2, GLUT1, PDHα1, and PDK (N=4). A negative control (no primary antibody) has been performed to confirm the specificity of each antibody.

	Gender	Age of diagnosis	Histological variant	TNM	Lesion size (cm)	BRAF mut
PTC-a	W	39	classical	pT1bN0M0	1.1	yes
PTC-b	W	61	classical	Pt3N0M0	1.2	yes
PTC-c	M	85	classical	pT4aN1aMO	3	yes
PTC-d	M	44	classical	Pt1N0M0	0.6	yes
PTC-e	W	58	classical (partially follicular)	pT1NxM0	1.4	yes

Protein	Name	DB number	PTC-a	PTC-b	PTC-c	PTC-d	PTC-e
SH3BP4	SH3-domain binding protein 4	A8K594	-2.9	-4.1	-5.1	-6.1	-9.5
IQGAP1	IQ motif containing GTPase activating protein 1	A4QPB0	1.5	2.4	1.6	1.6	1.9
KRT8	Keratin 8	F8VXB4	1.6	2.7	1.2	5.2	3.6
SERPINA1	Epididymis secretory sperm binding protein Li 44a	E9KL23	3.6	2.6	1.3	1.3	3.1
KRT7	Keratin 7	E7ES34	2.4	3.0	1.4	4.9	2.3
ATP5B	ATP synthase subunit beta (Fragment)	Q0QEN7	1.2	4.4	2.4	2.5	3.0
CTSB	Cathepsin B	A8K2H4	1.4	3.3	1.9	1.1	2.5
ACADVL	Very long-chain specific acyl-CoA dehydrogenase, mitochondrial	F5H2A9	1.5	2.1	2.1	2.2	2.9
HSPD1	Mitochondrial heat shock 60kD protein 1 variant 1	B3GQS7	1.9	3.7	2.8	3.5	4.2
RRBP1	p180/ribosome receptor	A7BI36	1.3	1.5	1.3	1.6	1.4
GAPDH	Glyceraldehyde-3-phosphate dehydrogenase	E7EUT4	1.1	1.6	1.2	1.3	1.7
ANXA5	Annexin 5	D6RBL5	1.2	2.1	1.1	4.2	2.9
SUCLG2	Succinate-CoA ligase [GDP-forming] subunit beta, mitochondrial	C9JVT2	2.1	5.3	2.0	1.9	4.8
AK2	Adenylate kinase 2, mitochondrial	F8W1A4	1.0	2.9	2.1	2.1	3.0
PHB2	Prohibitin-2	F5GY37	1.4	3.8	3.1	1.5	3.4
LONP1	Lon protease homolog, mitochondrial	B4DPX0	1.2	1.1	2.7	2.4	3.9
HADH2	3-hydroxyacyl-CoA dehydrogenase type-2	Q6IBS9	1.1	2.3	2.8	1.6	2.2
PHB	Prohibitin, isoform CRA_a	A8K401	2.2	3.2	1.9	1.5	1.9
NME1-NME2	Nucleoside diphosphate kinase	Q32Q12	1.1	2.8	1.8	1.5	2.4
PDHA1	Pyruvate dehydrogenase E1 component subunit alpha	A5YVE9	3.7	3.0	1.6	1.1	1.8
IVD	Isovaleryl Coenzyme A dehydrogenase	Q53XZ9	1.4	3.0	2.4	1.3	2.0
DECR1	2,4-dienoyl-CoA reductase, mitochondrial	B7Z6B8	1.6	2.6	4.6	1.0	2.3
PRDX3	Thioredoxin-dependent peroxide reductase, mitochondrial	E9PH29	1.5	2.9	1.8	2.3	1.8
HIBADH	3'-hydroxyisobutyrate dehydrogenase, mitochondrial	Q546Z2	1.1	4.9	2.5	1.6	2.9
/	60S ribosomal protein L6	Q9HBB3	1.2	1.7	1.7	1.2	3.5
/	Ribosomal protein L4 variant (Fragment)	Q59GY2	1.5	2.7	1.3	1.6	1.6
VDAC1	Voltage-dependent anion-selective channel protein 1	B3KTS5	2.0	4.6	3.0	2.7	2.7
KRT19	Keratin 19	C9JM50	3.6	5.0	3.2	3.1	3.4
CS	Citrate synthase	B4DJV2	2.0	2.4	1.2	2.0	2.3
/	UV excision repair protein RAD23 homolog B	B4DEA3	2.3	2.3	2.0	1.5	1.5
CRYZ	Quinone oxidoreductase	A6NN60	1.0	2.6	1.6	1.6	1.5
SOD2	Superoxide dismutase (Fragment)	Q7Z7M4	2.3	4.9	2.2	2.7	4.1
DCI	Dodecenoyl-Coenzyme A delta isomerase, isoform CRA_a	Q96DC0	1.4	2.4	2.5	1.8	3.1
MSN	MSN protein (Fragment)	Q6PJT4	2.0	2.2	1.2	2.0	1.1
EEF1G	Eukaryotic translation elongation factor 1 gamm	Q53YD7	1.2	2.2	1.1	2.4	1.3
RPL14	Ribosomal protein L14 variant	Q6IPH7	1.0	3.2	1.9	2.4	1.0
/	Epididymal secretory protein E1	B4DV10	2.3	4.9	3.9	1.5	3.7
RPL7A	Ribosomal protein L7a	Q5T8U4	1.2	1.2	1.3	1.3	1.4
C1QBP	Complement component 1, q subcomponent binding protein	A8K651	1.8	5.0	1.1	1.7	2.4
FN1	Fibronectin splice variant E (Fragment)	A6YID6	4.9	8.0	1.9	3.1	4.7
RAC1	Ras-related C3 botulinum toxin substrate 1	A4D2P1	1.1	1.1	1.4	6.3	2.6

PC	Pyruvate carboxylase	E9PS68	3.0	3.7	2.2	2.7	3.2
AKR1A1	Alcohol dehydrogenase [NADP(+)]	Q5T621	1.6	1.2	2.1	2.4	1.1
ETHE1	Ethylmalonic encephalopathy 1, isoform CRA_a	B2RCZ7	4.7	5.4	2.3	1.1	3.0
/	Cytosol aminopeptidase	B4DQG5	1.1	2.0	1.2	1.2	2.1
KRT7	Keratin 7	F8VZY5	2.2	2.5	1.5	5.0	2.8
HIBCH	3-hydroxyisobutyryl-CoA hydrolase, mitochondrial	B8ZZZ0	1.5	2.4	2.0	1.8	3.7
S100A11	S100 calcium binding protein A11	B2R5H0	2.1	2.9	1.6	2.2	1.3
/	Moderately similar to Cathepsin B	B4DL49	1.4	3.3	1.9	1.1	2.5
PRKAR2A	cAMP-dependent protein kinase type II-alpha regulatory subunit	Q9BUB1	1.3	1.6	3.1	5.3	1.3
/	Chaperonin containing TCP1, subunit 6A isoform a variant (Fragment)	Q59ET3	2.1	1.3	1.2	3.6	3.4
CTSH	Cathepsin H	Q6IBC3	2.4	8.2	3.8	2.2	3.7
PCCA	Propionyl Coenzyme A carboxylase, alpha polypeptide	B2RDE0	1.6	1.1	3.2	1.7	2.3
ECH1	Delta 3,5-delta 2,4-dienoyl-CoA isomerase, mitochondrial	B4DVS4	5.4	2.9	5.2	1.1	1.8
HLA-DRB1	MHC class II antigen	Q4ZJJ2	1.5	1.7	1.1	1.2	1.9
SARNP	SAP domain-containing ribonucleoprotein	F8VZQ9	2.4	1.8	1.0	2.0	3.8
HNRPDL	Heterogeneous nuclear ribonucleoprotein D-like	B4DTA2	1.8	3.5	1.8	1.4	1.8
CHCHD3	MICOS complex subunit	C9JRZ6	1.5	3.4	1.1	3.6	1.3
TPD52L2	Tumor protein D52-like 2	Q5U0E0	2.2	5.1	1.9	4.2	1.7
TPD52	Tumor protein D52	C9J502	1.5	2.4	1.5	2.5	2.4
HMGA2	High-mobility group AT-hook 2	Q1M183	4.3	2.3	4.6	5.0	3.3
SUCLG2	Succinate-CoA ligase subunit betaG2 (Fragment)	Q3ZCW5	2.2	4.6	5.9	1.5	4.8
FKBP1A	Peptidylprolyl isomerase	Q0VDC6	1.4	2.0	1.3	3.4	3.6
GGCT	Gamma-glutamylcyclotransferase	B8ZZN4	3.7	2.7	3.7	3.7	3.0
FAM162A	Uncharacterized protein FAM162A	F8W7Q4	2.2	6.9	2.9	1.7	3.3
UBA2	SUMO-1 activating enzyme subunit 2	B2RDF5	1.8	3.6	2.9	2.2	1.7
VDAC2	Voltage-dependent anion-selective channel protein 2	Q5JSD2	2.1	4.6	1.2	1.7	4.4
ARPC3	Actin related protein 2/3 complex subunit 3	Q2LE71	2.2	5.9	2.4	7.7	5.7
/	Sorting nexin 1 isoform a variant (Fragment)	Q59GU6	3.4	2.0	1.5	3.2	1.3
S100A13	S100 calcium binding protein A13, isoform CRA_a (Fragment)	D3DV53	2.3	2.2	1.3	2.5	1.6
THOC4	THO complex subunit 4	E9PB61	1.2	1.2	4.1	3.6	1.2
NHP2L1	NHP2 non-histone chromosome protein 2-like 1	Q6FHM6	3.8	1.1	3.3	2.1	3.4
CFI	Complement factor I	E7ETH0	2.4	2.2	3.8	1.3	1.7
/	Solute carrier family 25, member 24	B7ZB41	2.8	5.5	4.3	4.7	3.2
RPS27	Ribosomal protein S27	Q5T4L6	1.2	7.0	1.2	1.9	1.9
/	Poly [ADP-ribose] polymerase	B4E0E1	2.0	1.2	7.0	7.8	3.7
ATP5B	ATP synthase subunit beta	F8VPV9	1.2	4.4	2.4	2.5	3.0
SAMHD1	SAM domain-and HD domain-containing protein 1 variant (Fragment)	Q59H15	3.4	2.1	3.9	2.1	1.9
CMPK	Cytidylate kinase, isoform CRA_a	B2R6S5	4.6	1.3	1.0	1.2	3.2
PHB2	Prohibitin-2	B4DP75	1.4	3.8	3.1	1.5	3.4
RPL14	Ribosomal protein L14	A8K7N0	1.1	2.9	1.9	1.8	1.1
GGCT	Gamma-glutamylcyclotransferase	B8ZZK2	4.0	1.9	1.1	2.4	9.3
ATP5L	ATP synthase subunit g, mitochondrial	E9PN17	4.0	4.9	6.4	2.0	9.7

RPL17	Ribosomal protein L17	B4E3C2	1.2	1.4	5.8	8.6	8.2
TEAD3	TEAD3 protein (Fragment)	Q96G15	1.6	1.6	4.3	7.1	2.9

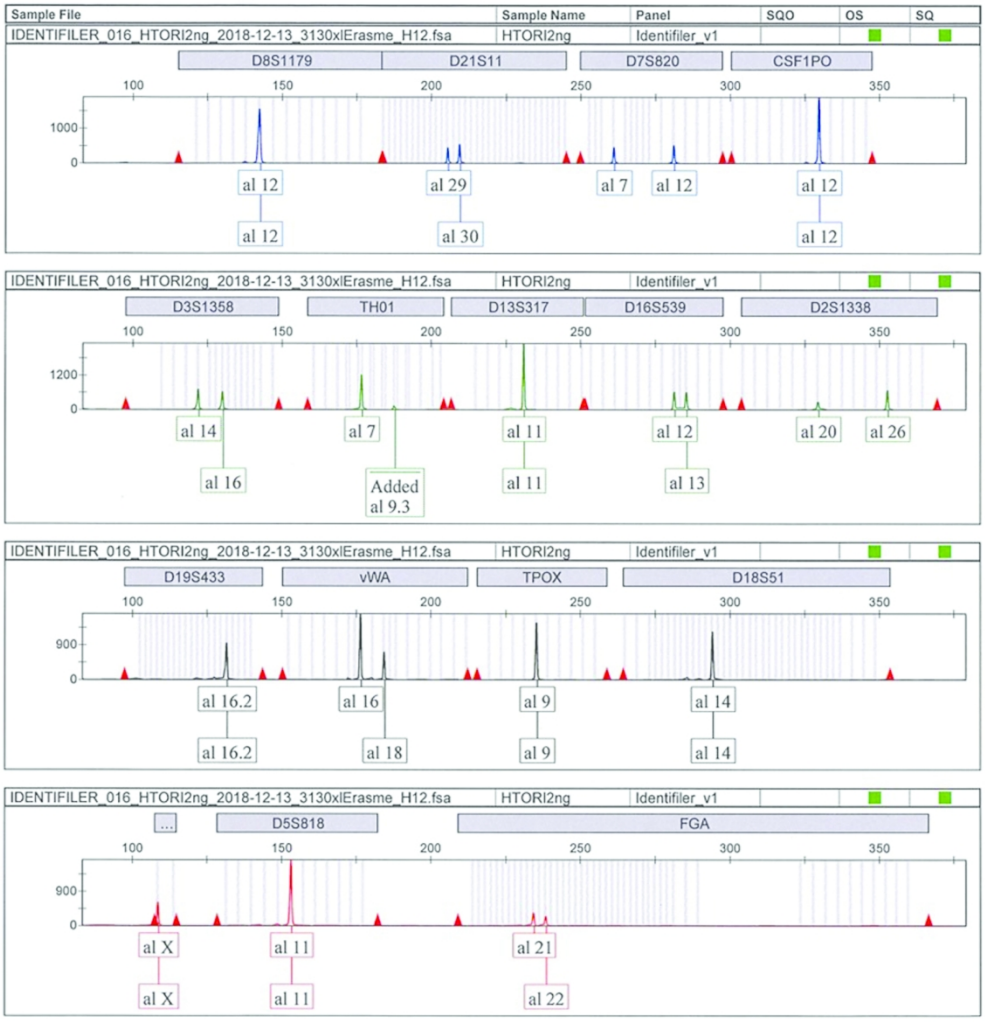

Figure S: DNA profiling by STR analysis of the HTori-3 cell line.